

Intrinsic nonlinear conductivity induced by quantum geometry in altermagnets and measurement of the in-plane Néel vector

Motohiko Ezawa¹

¹*Department of Applied Physics, The University of Tokyo, 7-3-1 Hongo, Tokyo 113-8656, Japan*

The z -component of the Néel vector is measurable by the anomalous Hall conductivity in altermagnets because time reversal symmetry is broken. On the other hand, it is a nontrivial problem how to measure the in-plane component of the Néel vector. We study the second-order nonlinear conductivity of a system made of the d -wave altermagnet with the Rashba interaction. It is shown that the quantum-metric induced nonlinear conductivity and the nonlinear Drude conductivity are proportional to the in-plane component of the Néel vector, and hence, the in-plane component of the Néel vector is measurable. We obtain analytic formulas of the quantum-metric induced nonlinear conductivity and the nonlinear Drude conductivity both for the longitudinal and transverse conductivities. The quantum-metric induced nonlinear conductivity diverges at the Dirac point, while the nonlinear Drude conductivity is always finite. Hence, the quantum-metric induced nonlinear conductivity is dominant at the Dirac point irrespective of the relaxation time.

Introduction: Altermagnets attracts much attention in the context of spintronics[1–3]. One of the reason is that the spin current can be generated[4–7] without using the spin-orbit interaction due to the momentum dependent band structure[1–3, 8, 9]. Indeed, momentum dependent band structures are observed by Angle-Resolved Photo-Emission Spectroscopy (ARPES)[10–14]. Although the net magnetization is zero in altermagnets, the z -component of the Néel vector is measurable with the aid of anomalous Hall effects due to the breaking of time-reversal symmetry[15–18].

Recently, there are many works on the nonlinear conductivity[19–31]. The second-order nonlinear conductivity $\sigma^{ab;c}$ is defined by $j^c = \sigma^{ab;c} E^a E^b$, where E^a is an applied electric field along the a direction and j^c is the current along the c direction. Especially, the nonlinear conductivity $\sigma^{ab;c}$ has three contributions: They are the quantum-metric induced nonlinear conductivity[29] $\sigma_{\text{Metric}}^{ab;c}$, the Berry curvature dipole induced nonlinear conductivity[32] $\sigma_{\text{Dipole}}^{ab;c}$, and the nonlinear Drude conductivity[33, 34] $\sigma_{\text{NLDrude}}^{ab;c}$. Here, quantum metric is defined by quantum distance with respect to the wave functions[35–37]. $\sigma_{\text{Dipole}}^{ab;c}$ and $\sigma_{\text{NLDrude}}^{ab;c}$ are proportional to τ and τ^2 , respectively, where τ is the electron relaxation time. They are extrinsic conductivities. On the other hand, $\sigma_{\text{Metric}}^{ab;c}$ is independent of τ , which is an intrinsic nonlinear conductivity. It is theoretically shown that $\sigma_{\text{Metric}}^{ab;c}$ is nonzero for the tilted Dirac system[28] and the Rashba system under in-plane magnetic field[38]. There is an experimental observation of $\sigma_{\text{Metric}}^{ab;c}$ in a Rashba system[39]. Furthermore, it is pointed out[40] that the leading term of the nonlinear conductivity is the third-order in d -wave altermagnets, where the direction of the Néel vector is assumed to be along the z direction.

In this paper, we study the second-order nonlinear conductivity in a system made of the d -wave altermagnet with the Rashba interaction without applying magnetic field. It is shown to be proportional to the in-plane component of the Néel vector in the d -wave altermagnet, and hence it is measurable by measuring the second-order nonlinear conductivity. We obtain analytic formula of the quantum-metric induced nonlinear conductivity and the nonlinear Drude con-

ductivity both for the longitudinal and transverse conductivities by using the first-order perturbation theory with respect to the magnitude of the altermagnetization. The quantum-metric induced nonlinear conductivity diverges at the Dirac point both for the longitudinal and transverse conductivities, while the nonlinear Drude conductivity is always finite. Hence, the quantum-metric induced nonlinear conductivity is dominant at the Dirac point irrespective of the relaxation time.

Nonlinear conductivity: The second-order nonlinear conductivity $\sigma^{ab;c}$ is expanded in terms of the electron relaxation time τ as[29]

$$\sigma^{ab;c} = \sigma_{\text{Metric}}^{ab;c} + \sigma_{\text{Dipole}}^{ab;c} + \sigma_{\text{NLDrude}}^{ab;c}, \quad (1)$$

where

$$\sigma_{\text{Metric}}^{ab;c} \propto \tau^0, \quad \sigma_{\text{Dipole}}^{ab;c} \propto \tau, \quad \sigma_{\text{NLDrude}}^{ab;c} \propto \tau^2. \quad (2)$$

We explain each term.

First, only the term $\sigma_{\text{Metric}}^{ab;c}$ survives in the dirty limit $\tau \rightarrow 0$, which is the intrinsic nonlinear conductivity. It is the quantum-metric induced nonlinear conductivity given by

$$\sigma_{\text{Metric}}^{ab;c}(\mu) = -\frac{e^3}{\hbar} \sum_n \int d^2k f_n \left(2 \frac{\partial G_n^{ab}}{\partial k_c} - \frac{1}{2} \left(\frac{\partial G_n^{bc}}{\partial k_a} + \frac{\partial G_n^{ac}}{\partial k_b} \right) \right), \quad (3)$$

where $f_n = 1/(\exp(E_n - \mu) + 1)$ is the Fermi distribution function for the band n , μ is the chemical potential, and G_n^{ab} is the band-energy normalized quantum metric or the Berry connection polarizability. It is given by[19, 20, 23, 24, 28, 29, 38]

$$G_n^{ab} = 2\text{Re} \sum_{m \neq n} \frac{A_{nm}^a(\mathbf{k}) A_{mn}^b(\mathbf{k})}{\varepsilon_n(\mathbf{k}) - \varepsilon_m(\mathbf{k})}, \quad (4)$$

with ε_n being the energy of the band n , and A_{nm}^a being the interband Berry connection

$$A_{nm}^a(\mathbf{k}) = i \langle \psi_n(\mathbf{k}) | \partial_{k_a} | \psi_m(\mathbf{k}) \rangle. \quad (5)$$

In what follows, we focus on the generic two-band system described by the Hamiltonian

$$H(\mathbf{k}) = h_0(\mathbf{k}) \sigma_0 + \sum_{j=x,y,z} h_j(\mathbf{k}) \sigma_j, \quad (6)$$

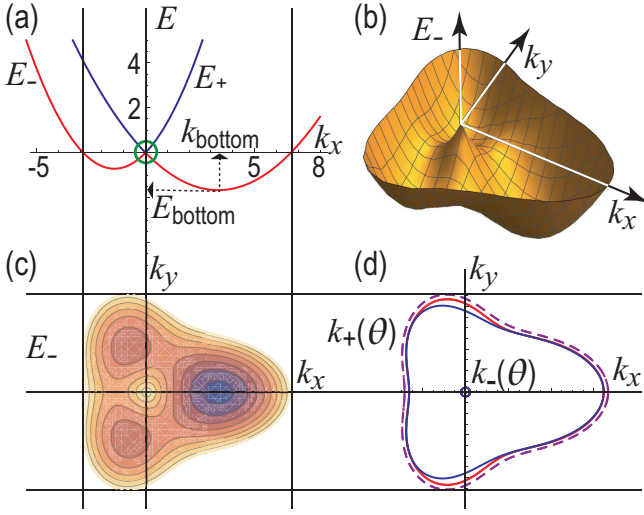


FIG. 1. (a) Energy spectrum $E_{\pm}(k_x, 0)$ in units of $E_0 = M\lambda^2/2\hbar^2$. The horizontal axis is k_x in units of $k_0 = M\lambda/2\hbar^2$. The green circle indicates the Dirac point. (b) Bird's eye's view of the lower energy E_- . (c) Contour plot of the lower energy E_- . (d) The tiny inner Fermi surface is $k_-(\theta)$ and the outer Fermi surfaces are $k_+(\theta)$ at $\mu = -0.2E_0$, where the blue curve is an analytical solution (18) based on the perturbation theory with respect to J , while the red curve is an analytic solution without perturbation. Purple dashed curve indicates the Fermi surface at $\mu = 0$. We have set $J = 0.1E_0/k_0^2$.

where σ_j is the Pauli matrix. The energy spectrum is given by

$$E_{\pm}(\mathbf{k}) = h_0(\mathbf{k}) \pm h(\mathbf{k}), \quad (7)$$

where $h(\mathbf{k}) \equiv \sqrt{\sum_{j=x,y,z} h_j^2(\mathbf{k})}$, by taking $n = \pm$ in Eq.(4). Eq.(4) is rewritten as[38]

$$G_-^{ab}(\mathbf{k}) = 2\text{Re} \frac{A_{-+}^a(\mathbf{k}) A_{+-}^b(\mathbf{k})}{\varepsilon_-(\mathbf{k}) - \varepsilon_+(\mathbf{k})} = -\frac{g^{ab}(\mathbf{k})}{2h(\mathbf{k})} \quad (8)$$

in terms of the quantum metric g^{ab} . For the two-band system it is given by[41–45]

$$g^{ab}(\mathbf{k}) = \frac{1}{2} \sum_{j=x,y,z} (\partial_{k_a} h_j) (\partial_{k_b} h_j). \quad (9)$$

Since this does not include $h_0(\mathbf{k})$, $G_-^{ab}(\mathbf{k})$ is independent of $h_0(\mathbf{k})$.

Second, $\sigma_{\text{Dipole}}^{ab;c}$ is the nonlinear transverse (Hall) conductivity induced by the Berry curvature dipole[32],

$$\sigma_{\text{Dipole}}^{ab;c}(\mu) = -\frac{e^3 \tau}{\hbar^2} \sum_n \int d^2 k f_n \left(\frac{\partial \Omega_n^{bc}}{\partial k_a} + \frac{\partial \Omega_n^{ac}}{\partial k_b} \right) \quad (10)$$

with the Berry curvature

$$\Omega_n^{ab} \equiv \partial_a A_{nn}^b(\mathbf{k}) - \partial_b A_{nn}^a(\mathbf{k}). \quad (11)$$

It is an extrinsic nonlinear conductivity, since it vanishes as $\tau \rightarrow 0$.

Third, $\sigma_{\text{NLDrude}}^{ab;c}$ is the nonlinear Drude conductivity[33],

$$\sigma_{\text{NLDrude}}^{ab;c}(\mu) = -\frac{e^3 \tau^2}{\hbar^3} \sum_n \int d^2 k f_n \frac{\partial^3 E_n}{\partial k_a \partial k_b \partial k_c}, \quad (12)$$

where E_n is the energy of the band n . It is also an extrinsic nonlinear conductivity.

Model: We consider a system made of the d -wave altermagnets with the Rashba interaction, whose Hamiltonian is given by[1–3]

$$H(\mathbf{k}) = \frac{\hbar^2 (k_x^2 + k_y^2)}{2M} \sigma_0 + \lambda (k_x \sigma_y - k_y \sigma_x) + J (k_x^2 - k_y^2) \mathbf{n} \cdot \boldsymbol{\sigma}, \quad (13)$$

where M is the effective mass, λ is the magnitude of the Rashba interaction, J is the magnitude of the d -wave altermagnetization, and \mathbf{n} is the Néel vector of the d -wave altermagnet. The Rashba interaction is introduced by placing an altermagnet on the substrate. The Rashba interaction breaks inversion symmetry, while the altermagnet term breaks time-reversal symmetry. Hence, the system breaks both inversion symmetry and time-reversal symmetry. Then, the nonlinear Drude conductivity and the quantum-metric induced nonlinear conductivity may emerge[29]. We assume $|J| < \hbar^2/(2M)$ so that the parabolic dispersion is positive for large $k = |\mathbf{k}|$.

The nonlinear conductivity $\sigma^{yy;x}$ is nonzero when the Néel vector is along the y direction $\mathbf{n} = (0, 1, 0)$, as we show later in Eqs.(23) and (24). We take $\mathbf{n} = (0, 1, 0)$ in the following. In this case, the energy is given by

$$E_{\pm}(\mathbf{k}) = \frac{\hbar^2 k^2}{2M} \pm \sqrt{(\lambda k_x + J(k_x^2 - k_y^2))^2 + \lambda^2 k_y^2}, \quad (14)$$

which is shown in Fig.1. The inversion symmetry with respect to k_x is broken for $J \neq 0$.

The energy along $k_y = 0$ is shown in Fig.1(a). Two energy spectra E_{\pm} touch at the Dirac point $k_x = k_y = 0$ and $E = 0$, which does not shift in the presence of altermagnetization J .

The energy (14) is minimized as

$$E_{\text{bottom}} = -\frac{M\lambda^2}{2(\hbar^2 - 2|J|M)} \quad (15)$$

at the band minimum point

$$k_x^{\text{bottom}} = \frac{M\lambda}{\hbar^2 - 2|J|M}, \quad k_y^{\text{bottom}} = 0, \quad (16)$$

as shown in Fig.1(a).

Quantum-metric induced nonlinear conductivity: We study the longitudinal nonlinear conductivity induced by quantum metric. $\partial G_n^{xx}/\partial k_x$ is antisymmetric with respect to k_x for $J = 0$. However, this antisymmetry is broken for $J \neq 0$. In addition, there is no inversion symmetry in the energy (14) for $J \neq 0$. As a result, $\sigma_{\text{Metric}}^{xx;x}$ becomes finite for $J \neq 0$. $\sigma_{\text{Metric}}^{xx;x}$ is numerically calculated and is shown in Fig.2(a). The sign of the conductivity is reversed when the sign of J is reversed. It diverges at the Dirac point ($\mu = 0$) as

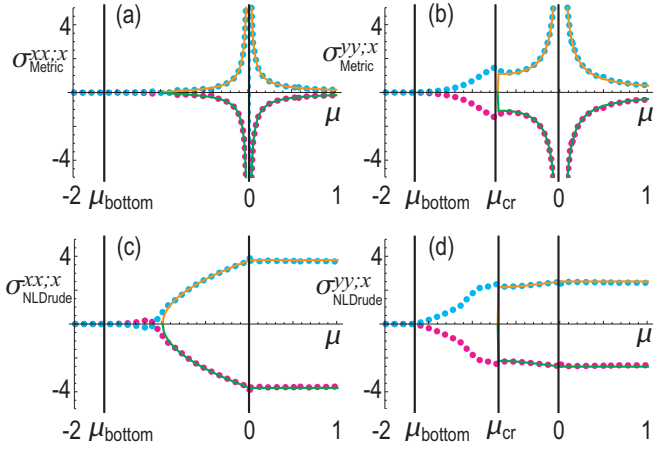


FIG. 2. (a) Quantum-metric induced longitudinal conductivity $\sigma_{\text{Metric}}^{xx;x}$ in units of $e^3/(\hbar E_0 k_0)$. (b) Quantum-metric induced transverse conductivity $\sigma_{\text{Metric}}^{yy;x}$ in units of $e^3/(\hbar E_0 k_0)$. (c) Longitudinal nonlinear Drude conductivity $\sigma_{\text{NLDrude}}^{xx;x}$ in units of $e^3 \tau^2 E_0/(\hbar^3 k_0)$. (d) Transverse nonlinear Drude conductivity $\sigma_{\text{NLDrude}}^{yy;x}$ in units of $e^3 \tau^2 E_0/(\hbar^3 k_0)$. The horizontal axis is the chemical potential μ in units of E_0 . Red dots indicate numerically obtained results by setting $J = 0.1E_0/k_0^2$, while cyan dots indicate numerically obtained results by setting $J = -0.1E_0/k_0^2$. Green curves indicate analytically obtained results by setting $J = 0.1E_0/k_0^2$, while orange curves indicate analytically obtained results by setting $J = -0.1E_0/k_0^2$. See the definition of E_0 and k_0 in the caption of Fig.1. We have set $\mu_{\text{bottom}} = E_{\text{bottom}}$ with Eq.(15) and μ_{cr} is defined by Eq.(19).

shown in Fig.2(a). $\sigma_{\text{Metric}}^{xx;x}$ is linear as a function of J as shown in Fig.3(a).

We analytically calculate $\sigma_{\text{Metric}}^{xx;x}$ based on the first-order perturbation theory in J , which is valid for $2M|J| \ll \hbar^2$. Actually, the conductivity is almost linear for $2M|J| < \hbar^2$ as shown in Fig.3(a). The energy (14) is expanded as

$$E_-(\mathbf{k}) = -\lambda k + Jk^2 \cos \theta \cos 2\theta + \frac{\hbar^2 k^2}{2M}, \quad (17)$$

where we have introduced the polar coordinate of the momentum, $k_x = k \cos \theta$ and $k_y = k \sin \theta$.

The Fermi surface is numerically obtained and shown in Fig.1(d). In the vicinity of the Dirac point, there are two Fermi surfaces. In the first-order of J , the Fermi surfaces at $E_- = \mu$ are determined by $k(\theta) = k_{\pm}(\theta)$ with

$$k_{\pm}(\theta) = \frac{\lambda \pm \sqrt{\frac{2\mu\hbar^2}{M} + \lambda^2 - 2\mu J(\cos \theta + \cos 3\theta)}}{\frac{\hbar^2}{M} - J(\cos \theta + \cos 3\theta)}, \quad (18)$$

which is valid for

$$\mu > -\frac{M\lambda^2}{2(\hbar^2 + 2M|J|)} \equiv \mu_{\text{cr}}. \quad (19)$$

The quantum-metric induced nonlinear conductivity is calculated as

$$\sigma_{\text{Metric}}^{xx;x} = -\frac{e^3}{\hbar} \int d^2k f_n \frac{\partial G_-^{xx}}{\partial k_x} = \int_{k_-}^{k_+} k dk \int_0^{2\pi} d\theta \frac{\partial G_-^{xx}}{\partial k_x}. \quad (20)$$

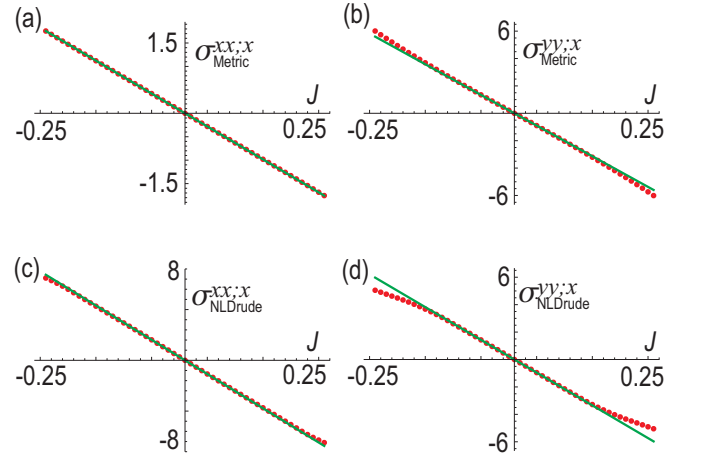


FIG. 3. J dependence of the nonlinear conductivity. (a) $\sigma_{\text{Metric}}^{xx;x}$. (b) $\sigma_{\text{Metric}}^{yy;x}$. (c) $\sigma_{\text{NLDrude}}^{xx;x}$ and (d) $\sigma_{\text{NLDrude}}^{yy;x}$. Their units are given in the caption of Fig.2. Red dots indicate numerically obtained results, while green lines indicate analytically obtained results. The horizontal axis is J in units of k_0^2 . We have set $\mu = -0.2E_0$. See the definitions of E_0 and k_0 in the caption of Fig.1.

Up to the first order of J , we have

$$\frac{\partial G_-^{xx}}{\partial k_x} = \frac{5 \cos \theta \sin^2 \theta}{2\lambda k^3} + J \sin^2 \theta \frac{35 \cos 4\theta - 10 \cos 2\theta - 9}{8\lambda^2 k^2}. \quad (21)$$

By integrating it over k , we have

$$\sigma_{\text{Metric}}^{xx;x} = -\frac{e^3}{\hbar} \int_0^{2\pi} d\theta \frac{5 \cos \theta \sin^2 \theta}{6\lambda} \left(\frac{1}{k_-^2} - \frac{1}{k_+^2} \right) + J \sin^2 \theta \frac{35 \cos 4\theta - 10 \cos 2\theta - 9}{16\lambda^2 k^3} \left(\frac{1}{k_-} - \frac{1}{k_+} \right). \quad (22)$$

It is analytically calculated as

$$\sigma_{\text{Metric}}^{xx;x} = -\frac{e^3 \pi J \sqrt{2\mu\hbar^2 + M\lambda^2}}{\hbar 2\mu^2 \sqrt{M}\lambda} \quad (23)$$

for $\mu < 0$, and

$$\sigma_{\text{Metric}}^{xx;x} = -\frac{e^3 \pi J}{\hbar 2\mu\lambda} \propto J \quad (24)$$

for $\mu > 0$. It is proportional to J . Hence, J is measurable if the magnitude of λ is known. The formula well fits the numerical result as shown in Fig.2(a).

Angle dependence: Both $\sigma_{\text{Metric}}^{xx;x}$ and $\sigma_{\text{NLDrude}}^{xx;x}$ are zero when the Néel vector is along the x direction $\mathbf{n} = (1, 0, 0)$ or the Néel vector is along the z direction $\mathbf{n} = (0, 0, 1)$.

First, we study the angle dependence of the Néel vector along the y - x plane by setting $\mathbf{n} = (\sin \Phi, \cos \Phi, 0)$. In the first-order of J , we analytically obtain $\sigma_{\text{Metric}}^{xx;x}(\Phi) = \sigma_{\text{Metric}}^{xx;x}(0) \cos \Phi$ and $\sigma_{\text{NLDrude}}^{xx;x}(\Phi) = \sigma_{\text{NLDrude}}^{xx;x}(0) \cos \Phi$. Next, we study the angle dependence of the Néel vector along the y - z plane by setting $\mathbf{n} = (0, \cos \Theta, \sin \Theta)$. In the first-order

of J , we analytically obtain $\sigma_{\text{Metric}}^{xx;x}(\Theta) = \sigma_{\text{Metric}}^{xx;x}(0) \cos \Theta$ and $\sigma_{\text{NLDrude}}^{xx;x}(\Theta) = \sigma_{\text{NLDrude}}^{xx;x}(0) \cos \Theta$.

Nonlinear Hall conductivity: Next, we calculate the quantum-metric induced nonlinear Hall conductivity.

First, we have $\sigma_{\text{Metric}}^{xx;y} = 0$, because

$$2 \frac{\partial G_n^{xx}}{\partial k_y} - \frac{\partial G_n^{xy}}{\partial k_x} \propto k_y, \quad (25)$$

and its integration over k_y vanishes.

On the other hand, we obtain a nontrivial result for $\sigma_{\text{Metric}}^{yy;x}$. The μ dependence of $\sigma_{\text{Metric}}^{yy;x}$ is numerically obtained and shown in Fig.2(b). It is linear as a function of J as in Fig.3(b). It is analytically calculated up to the first order in J as

$$\sigma_{\text{Metric}}^{yy;x} = -\frac{e^3 \tau}{\hbar^2} \frac{\pi J (\mu \hbar^2 - 5M\lambda^2)}{4\mu\lambda^2 \sqrt{M} \sqrt{2\mu\hbar^2 + M\lambda^2}} \propto J \quad (26)$$

for $\mu < 0$ and

$$\sigma_{\text{Metric}}^{yy;x} = -\frac{e^3 \tau}{\hbar^2} \frac{5\pi J}{2\mu\lambda} \propto J \quad (27)$$

for $\mu > 0$.

Nonlinear longitudinal Drude conductivity: The μ dependence of $\sigma_{\text{Drude}}^{xx;x}$ is shown in Fig.2(c). It is linear as a function of J as shown in Fig.3(c). It is analytically calculated up to the first order in J as

$$\sigma_{\text{NLDrude}}^{xx;x} = -\frac{e^3 \tau^2}{\hbar^5} 6\pi J \sqrt{M} \sqrt{2\mu\hbar^2 + M\lambda^2} \propto J \quad (28)$$

for $\mu < 0$ and

$$\sigma_{\text{NLDrude}}^{xx;x} = -\frac{e^3 \tau^2}{\hbar^5} 6\pi J M \lambda \propto J \quad (29)$$

for $\mu > 0$.

Nonlinear transverse Drude conductivity: The μ dependence of $\sigma_{\text{Drude}}^{yy;x}$ is shown in Fig.2(d). It is linear as a function of J as in Fig.3(d). It is analytically calculated up to the first order in J as

$$\sigma_{\text{NLDrude}}^{yy;x} = -\frac{e^3 \tau^2}{\hbar^5} \frac{2\pi J \sqrt{M} (3\mu\hbar^2 + 2M\lambda^2)}{\sqrt{2\mu\hbar^2 + M\lambda^2}} \propto J \quad (30)$$

for $\mu < 0$

$$\sigma_{\text{NLDrude}}^{yy;x} = -\frac{e^3 \tau^2}{\hbar^5} 4\pi J M \lambda \propto J \quad (31)$$

for $\mu > 0$.

Discussions: We have investigated the second-order nonlinear conductivity of a system made of the d -wave altermagnet with the Rashba interaction. We have focused on the problem to measure the direction of the Néel vector.

$\sigma_{\text{Metric}}^{xx;x}$, $\sigma_{\text{Metric}}^{yy;x}$, $\sigma_{\text{NLDrude}}^{xx;x}$ and $\sigma_{\text{NLDrude}}^{yy;x}$ are proportional to J and have the same sign. Hence, J is measurable irrespective of τ .

$\sigma_{\text{Metric}}^{xx;x}$ and $\sigma_{\text{Metric}}^{yy;x}$ diverge at the Dirac point $\mu = 0$, while $\sigma_{\text{NLDrude}}^{xx;x}$ and $\sigma_{\text{NLDrude}}^{yy;x}$ are finite. Hence, $\sigma_{\text{Metric}}^{xx;x}$ and $\sigma_{\text{Metric}}^{yy;x}$ are dominant comparing with $\sigma_{\text{NLDrude}}^{xx;x}$ and $\sigma_{\text{NLDrude}}^{yy;x}$ in the vicinity of the Dirac point.

In addition, the quantum-metric induced nonlinear conductivity $\sigma_{\text{Metric}}^{xx;x}$ and $\sigma_{\text{Metric}}^{yy;x}$ become significant in the dirty metal $\tau \rightarrow 0$. In this dirty regime, $\sigma_{\text{Metric}}^{xx;x}$ and $\sigma_{\text{Metric}}^{yy;x}$ are dominant comparing with $\sigma_{\text{NLDrude}}^{xx;x}$ and $\sigma_{\text{NLDrude}}^{yy;x}$ even away from the Dirac point.

The x -component of the Néel vector is measurable by observing $\sigma_{\text{Metric}}^{yy;y}$. By combining the results of $\sigma_{\text{Metric}}^{xx;x}$ and $\sigma_{\text{Metric}}^{yy;y}$, the in-plane component of the Néel vector is measurable.

The Berry-curvature dipole induced nonlinear Hall effect is another result on the nonlinear conductivity. In the present system, the Berry curvature is exactly zero except at the Dirac point because the system is gapless at the Dirac point. Hence, there is no Berry-curvature dipole induced nonlinear Hall effect in the present system.

This work is supported by CREST, JST (Grants No. JPMJCR20T2) and Grants-in-Aid for Scientific Research from MEXT KAKENHI (Grant No. 23H00171).

-
- [1] L. Smejkal, A. H. MacDonald, J. Sinova, S. Nakatsuji and T. Jungwirth, Anomalous Hall antiferromagnets, *Nat. Rev. Mater.* 7, 482 (2022).
 [2] L. Smejkal, J. Sinova, and T. Jungwirth, Beyond Conventional Ferromagnetism and Antiferromagnetism: A Phase with Non-relativistic Spin and Crystal Rotation Symmetry, *Phys. Rev. X*, 12, 031042 (2022).
 [3] Libor Šmejkal, Jairo Sinova, and Tomas Jungwirth, Emerging Research Landscape of Altermagnetism, *Phys. Rev. X* 12, 040501 (2022).
 [4] Makoto Naka, Satoru Hayami, Hiroaki Kusunose, Yuki Yanagi, Yukitoshi Motome and Hitoshi Seo, Spin current generation in

- organic antiferromagnets, *Nat. Com.* 10, 4305 (2019).
 [5] Rafael Gonzalez-Hernandez, Libor Šmejkal, Karel Vborn, Yuta Yahagi, Jairo Sinova, Tomš Jungwirth, and Jakub Železn. Efficient electrical spin splitter based on nonrelativistic collinear antiferromagnetism, *Phys. Rev. Lett.*, 126:127701, (2021).
 [6] M Naka, Y Motome, and H Seo, Perovskite as a spin current generator. *Phys. Rev. B*, 103, 125114, (2021).
 [7] Arnab Bose, Nathaniel J. Schreiber, Rakshit Jain, Ding-Fu Shao, Hari P. Nair, Jiabin Sun, Xiyue S. Zhang, David A. Muller, Evgeny Y. Tsymbal, Darrell G. Schlom & Daniel C. Ralph, Tilted spin current generated by the collinear antiferromagnet ruthenium dioxide, *Nature Electronics* 5, 267 (2022).

- [8] K.-H. Ahn, A. Hariki, K.-W. Lee, and J. Kunes, Antiferromagnetism in RuO₂ as d-wave Pomeranchuk instability, *Phys. Rev. B* 99, 184432 (2019).
- [9] S. Hayami, Y. Yanagi, and H. Kusunose, Momentum-Dependent Spin Splitting by Collinear Antiferromagnetic Ordering, *J. Phys. Soc. Jpn.* 88, 123702 (2019).
- [10] J. Krempask, L. Šmejkal, S. W. D'Souza, M. Hajlaoui, G. Springholz, K. Uhlov F. Alarab, P. C. Constantinou, V. Strocov, D. Usanov, W. R. Pudelko, R. Gonzez-Herndez, A. Birk Hellenes, Z. Jansa, H. Reichlov Z. Šob, R. D. Gonzalez Betancourt, P. Wadley, J. Sinova, D. Kriegner, J. Min, J. H. Dil and T. Jungwirth, Altermagnetic lifting of Kramers spin degeneracy, *Nature* 626, 517 (2024).
- [11] Suyoung Lee, Sangjae Lee, Saegyeol Jung, Jiwon Jung, Donghan Kim, Yeonjae Lee, Byeongjun Seok, Jaeyoung Kim, Byeong Gyu Park, Libor Šmejkal, Chang-Jong Kang, Changyong Kim, Broken Kramers Degeneracy in Altermagnetic MnTe, *Phys. Rev. Lett.* 132, 036702 (2024).
- [12] O. Fedchenko, J. Minar, A. Akashdeep, S.W. D'Souza, D. Vasilyev, O. Tkach, L. Odenbreit, Q.L. Nguyen, D. Kutnyakhov, N. Wind, L. Wenthous, M. Scholz, K. Rossnagel, M. Hoesch, M. Aeschlimann, B. Stadtmueller, M. Klauui, G. Schoenhense, G. Jakob, T. Jungwirth, L. Smejkal, J. Sinova, H. J. Elmers, Observation of time-reversal symmetry breaking in the band structure of altermagnetic RuO₂, *Science Advances* 10,5 (2024) DOI: 10.1126/sciadv.adj4883.
- [13] T. Osumi, S. Souma, T. Aoyama, K. Yamauchi, A. Honma, K. Nakayama, T. Takahashi, K. Ohgushi, and T. Sato, Observation of a giant band splitting in altermagnetic MnTe, *Phys. Rev. B* 109, 115102 (2024)
- [14] Zihan Lin, Dong Chen, Wenlong Lu, Xin Liang, Shiyu Feng, Kohei Yamagami, Jacek Osiecki, Mats Leandersson, Balasubramanian Thiagarajan, Junwei Liu, Claudia Felser, Junzhang Ma, Observation of Giant Spin Splitting and d-wave Spin Texture in Room Temperature Altermagnet RuO₂, arXiv:2402.04995.
- [15] Amar Fakhredine, Raghottam M. Sattigeri, Giuseppe Cuono, and Carmine Autieri, Interplay between altermagnetism and nonsymmorphic symmetries generating large anomalous Hall conductivity by semi-Dirac points induced anticrossings, *Phys. Rev. B* 108, 115138 (2023).
- [16] Teresa Tschirner, Philipp Keler, Ruben Dario Gonzalez Betancourt, Tommy Kotte, Dominik Kriegner, Bernd Buechner, Joseph Dufouleur, Martin Kamp, Vedran Jovic, Libor Smejkal, Jairo Sinova, Ralph Claessen, Tomas Jungwirth, Simon Moser, Helena Reichlova, Louis Veyrat, Saturation of the anomalous Hall effect at high magnetic fields in altermagnetic RuO₂, *APL Mater.* 11, 101103 (2023)
- [17] Toshihiro Sato, Sonia Haddad, Ion Cosma Fulga, Fakhre F. Asaad, Jeroen van den Brink, Altermagnetic anomalous Hall effect emerging from electronic correlations, *Phys. Rev. Lett.* 133, 086503 (2024)
- [18] Miina Leivisk Javier Rial, Anton Badura, Rafael Lopes Seeger, Ismaa Kounta, Sebastian Beckert, Dominik Kriegner, Isabelle Joumard, Eva Schmoranzero Jairo Sinova, Olena Gomonay, Andy Thomas, Sebastian T. B. Goennenwein, Helena Reichlov Libor Smejkal, Lisa Michez, Tom Jungwirth, Vincent Baltz, Anisotropy of the anomalous Hall effect in the altermagnet candidate Mn₅Si₃ films, *Phys. Rev. B* 109, 224430 (2024)
- [19] Y. Gao, S. A. Yang, and Q. Niu, Field induced positional shift of Bloch electrons and its dynamical implications, *Phys. Rev. Lett.* 112, 166601 (2014).
- [20] H. Liu, J. Zhao, Y.-X. Huang, W. Wu, X.-L. Sheng, C. Xiao, and S. A. Yang, Intrinsic second-order anomalous Hall effect and its application in compensated antiferromagnets, *Phys. Rev. Lett.* 127, 277202 (2021).
- [21] Y. Michishita and N. Nagaosa, Dissipation and geometry in nonlinear quantum transports of multiband electronic systems, *Phys. Rev. B* 106, 125114 (2022).
- [22] H. Watanabe and Y. Yanase, Nonlinear electric transport in odd-parity magnetic multipole systems: Application to Mn-based compounds, *Phys. Rev. Res.* 2, 043081 (2020)
- [23] C. Wang, Y. Gao, and D. Xiao, Intrinsic nonlinear Hall effect in antiferromagnetic tetragonal cumnna, *Phys. Rev. Lett.* 127, 277201 (2021).
- [24] C. Wang, Y. Gao, and D. Xiao, Intrinsic nonlinear Hall effect in antiferromagnetic tetragonal cumnna, *Phys. Rev. Lett.* 127, 277201 (2021).
- [25] R. Oiwa and H. Kusunose, Systematic analysis method for nonlinear response tensors, *J. Phys. Soc. Jpn.* 91, 014701 (2022).
- [26] A. Gao, Y.-F. Liu, J.-X. Qiu, B. Ghosh, T.V. Trevisan, Y. Onishi, C. Hu, T. Qian, H.-J. Tien, S.-W. Chen et al., Quantum metric nonlinear Hall effect in a topological antiferromagnetic heterostructure, *Science* 381, eadf1506 (2023).
- [27] N. Wang, D. Kaplan, Z. Zhang, T. Holder, N. Cao, A. Wang, X. Zhou, F. Zhou, Z. Jiang, C. Zhang et al., Quantum metric-induced nonlinear transport in a topological antiferromagnet, *Nature (London)* 621, 487 (2023).
- [28] Kamal Das, Shibali Lahiri, Rhonald Burgos Atencia, Dimitrie Culcer, and Amit Agarwal, Intrinsic nonlinear conductivities induced by the quantum metric, *Phys. Rev. B* 108, L201405 (2023)
- [29] Daniel Kaplan, Tobias Holder and Binghai Yan, Unification of Nonlinear Anomalous Hall Effect and Nonreciprocal Magnetoresistance in Metals by the Quantum Geometry, *Phys. Rev. Lett.* 132, 026301 (2024)
- [30] YuanDong Wang, ZhiFan Zhang, Zhen-Gang Zhu, and Gang Su, Intrinsic nonlinear Ohmic current, *Phys. Rev. B* 109, 085419 (2024)
- [31] Longjun Xiang, Bin Wang, Yadong Wei, Zhenhua Qiao, and Jian Wang, Linear displacement current solely driven by the quantum metric, *Phys. Rev. B* 109, 115121 (2024)
- [32] I. Sodemann and L. Fu, Quantum nonlinear Hall effect induced by Berry curvature dipole in time-reversal invariant materials, *Phys. Rev. Lett.* 115, 216806 (2015).
- [33] D. Kaplan, T. Holder, and B. Yan, Unifying semiclassics and quantum perturbation theory at nonlinear order, *SciPost Phys.* 14, 082 (2023)
- [34] T. Ideue, K. Hamamoto, S. Koshikawa, M. Ezawa, S. Shimizu, Y. Kaneko, Y. Tokura, N. Nagaosa, and Y. Iwasa, Bulk rectification effect in a polar semiconductor, *Nat. Phys.* 13, 578 (2017).
- [35] J. P. Provost and G. Vallee, Riemannian structure on manifolds of quantum states, *Comm. Math. Phys.* 76, 289 (1980).
- [36] Yu-Quan Ma, Shu Chen, Heng Fan, and Wu-Ming Liu, Abelian and non-Abelian quantum geometric tensor, *Phys. Rev. B* 81, 245129 (2010).
- [37] R. Resta, The insulating state of matter: a geometrical theory, *Eur. Phys. J. B* 79, 121 (2011)
- [38] Maria Teresa Mercaldo, Mario Cuoco, and Camine Ortix, Non-linear planar magnetotransport as a probe of the quantum geometry of topological surface states, arXiv:2408.09543
- [39] Giacomo Sala, et.al., The quantum metric of electrons with spin-momentum locking, arXiv:2407.06659
- [40] Yuan Fang, Jennifer Cano, and Sayed Ali Akbar Ghorashi, Quantum Geometry Induced Nonlinear Transport in Altermagnets, *Phys. Rev. Lett.* 133, 106701 (2024)
- [41] Yugo Onishi and Liang Fu, Fundamental Bound on Topological Gap, *Phys. Rev. X* 14, 011052 (2024)

- [42] Shunji Matsuura and Shinsei Ryu, Momentum space metric, nonlocal operator, and topological insulators, *Phys. Rev. B* 82, 245113 (2010)
- [43] G. von Gersdorff and W. Chen, Measurement of topological order based on metric-curvature correspondence, *Phys. Rev. B* 104, 195133 (2021).
- [44] Wei Chen, Quantum geometrical properties of topological materials, arXiv:2406.15145
- [45] Motohiko Ezawa, Analytic approach to quantum metric and optical conductivity in Dirac models with parabolic mass in arbitrary dimensions, arXiv:2408.02951